Arvind Nayak
Department of Mechanical Engineering,
Indian Institute of Science,
Bengaluru 560012, India

Poornakanta Handral
Department of Mechanical Engineering,
Indian Institute of Science,
Bengaluru 560012, India

Ramsharan Rangarajan[1]
Department of Mechanical Engineering,
Indian Institute of Science,
Bengaluru 560012, India
e-mail: rram@iisc.ac.in

Shape Control for the Elastica Through Load Optimization

Flexible elastic beams can function as dexterous manipulators at multiple length-scales and in various niche applications. As a step toward achieving controlled manipulation with flexible structures, we introduce the problem of approximating desired quasi-static deformations of a flexible beam, modeled as an elastica, by optimizing the loads applied. We presume the loads to be concentrated, with the number and nature of their application prescribed based on design considerations and operational constraints. For each desired deformation, we pose the problem of computing the requisite set of loads to mimic the target shape as one of optimal approximations. In the process, we introduce a novel generalization of the forward problem by considering the inclinations of the loads applied to be functionals of the solution. This turns out to be especially beneficial when analyzing tendon-driven manipulators. We demonstrate the shape control realizable through load optimization using a diverse set of experiments. [DOI: 10.1115/1.4041678]

1 Introduction

We consider the problem of computing an optimal set of concentrated loads acting at prescribed locations along a flexible elastic beam, with the objective of realizing a desired deformed shape at static equilibrium. Our motivation to study this problem lies in the context of controlling shapes of flexible arms to serve as manipulators in robotics applications. Such control helps to transform a passive elastic beam into an active flexible manipulator that can be used, for instance, to inspect a cluttered environment, to mimic a grasping pose in an assistive glove, or to steer a minimally invasive medical instrument [1,2].

We presume from the outset that the arm we seek to control is a slender structure that can undergo large displacements and rotations while incurring small strains. Consequently, linear beam theories are inadequate and a linear relationship between loads and displacements is unrealistic in the typical regime of operation for flexible manipulators. Instead, we model the arm as an *elastica*. Hence, the material response remains linear, which, in this case, implies a bending moment proportional to the local curvature. On the other hand, the kinematics is nonlinear and curvatures are computed without approximation in the model [3].

The forward problem of computing the deformation of a flexible arm modeled as an elastica for a prescribed set of loads, though nonlinear, is reasonably straightforward to resolve. Solutions expressed in terms of elliptic integrals have been derived for various combinations of loads, moments and boundary conditions [4–8]. Numerical algorithms to compute approximate solutions, predominantly based on the shooting method, can be adopted as well [9–12]. Though these solutions are often presented for an end load/moment, it is conceivable that the techniques used, especially the numerical algorithms, can be extended with some tedium to the case of multiple loads. We revisit the forward problem in Sec. 2, where we consider loads whose inclinations are general functionals of the elastica solution. Such a generalization appears to be novel, and turns out to be very useful for analyzing a broad class of loading scenarios including tendon-driven manipulators discussed in Sec. 4, see Fig. 1.

The shape control problem that we introduce in Sec. 3 is more challenging and seems to have largely escaped attention in the literature. The main difficulty arises from the prescribed nature of the loading. To wit, if a distributed loading is permitted, shape control becomes trivial—for a desired deformation, simply find the out-of-balance forces/moments required to maintain static equilibrium. In fact, such a scenario, though unrealistic in practice, enables any desired deformation to be achieved. In contrast, we assume the loads to be concentrated, and consider their number to be finite and their locations to be given. Such restrictions inevitably arise from application-specific design considerations. Then, it is not clear if a desired deformation is even achievable. It is in fact generally the case that a target deformation can only be approximated and not reproduced exactly. This observation highlights that our shape control problem is not just an inverse problem for the elastica [13,14], but one of optimal approximations.

Our approach to shape control for the elastica consists of posing an optimization problem, where the parameters we seek are the loads to be imposed on the arm and the objective functional is defined to minimize deviations of the realized equilibrium configuration from the desired one. The proposed numerical algorithm for computing these loads falls under the category of ordinary differential equation-constrained optimization methods [15], with the distinctive feature that the underlying state equation is nonlinear. These aspects clearly distinguish our approach from control algorithms in conventional robotics applications where the kinematics

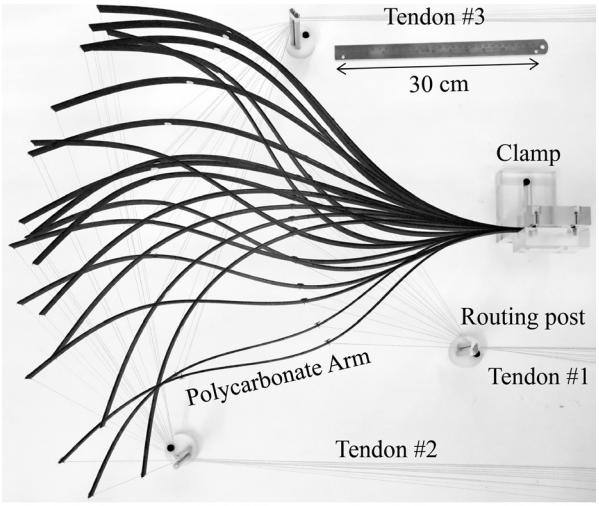

Fig. 1 An experimental realization demonstrating the manipulation of a flexible polycarbonate beam using three tendon loads

[1]Corresponding author.

Contributed by the Applied Mechanics Division of ASME for publication in the Journal of Applied Mechanics. Manuscript received September 5, 2018; final manuscript received October 4, 2018; published online November 2, 2018. Assoc. Editor: Yihui Zhang.

mainly involves a combination of algebraic and trigonometric relationships. We also draw a distinction between the load optimization problem for shape control introduced here and that of shape optimization for beams [16], where for example, the thickness or cross section is tuned to achieve a desired compliance.

We resolve the load optimization problem by explicitly computing sensitivities of elastica solutions to each of the imposed loads, which in turn helps to identify descent directions in numerical algorithms used to minimize the objective. In particular, we provide the equations satisfied by sensitivity fields, and discuss approximating elastica solutions and their sensitivities with the finite element method. We also highlight intricacies that arise when optimizing configuration-dependent loads where the direction of loading depends explicitly on the solution. In fact, the two most commonly used types of actuation in flexible robotics, namely, pressure-driven and tendon-driven mechanisms, fall under this category.

1.1 Related Literature. It is generally well recognized that the elastica serves as a useful model for planar flexible manipulators [17–20]. Similarly, in three dimensions, geometrically nonlinear rod models have been adopted to compute the forward kinematics of robots with slender continuum backbones [21,22], although simpler models invoking constant curvature approximations are far more prevalent [23,24]. With the intention of capturing macroscopic geometric features, conventional (hyperredundant) robots consisting of a large number of rigid links and actuators have even been approximated by continuum models such as the elastica [25]. As illustrated by the study in Ref. [26], however, drawing analogies between the mechanics of a serpentine hyperredundant robot and a continuum arm is an intricate matter.

While we envision employing a flexible arm as a robotic device by contorting it to a desired shape, other modalities are possible as well. As considered in Refs. [18] and [27], the arm can be used to deliver a payload to a desired location. It is possible to induce snap-through instabilities to harness the rapid release of energy for devising autonomous behavior [28]. A common theme underlying such modalities is the instability of an elastic arch subjected to a transverse load [29,30]. A snap-through induced by varying the end conditions transforms the structure into a "catapult" [31]. A similar principle is exploited in pole vaulting as well [32]. Snap-through and pull-in instabilities have also been used for designing devices in microelectromechanical systems [33].

The method of actuation plays a decisive role in the design and operation of flexible manipulators [34]. Our work here is targeted toward controlling tendon-driven arms, which offer the crucial benefit of isolating the actuation mechanism from the manipulator itself, thereby making the manipulator light and portable. Among alternative mechanisms, pneumatic/fluidic actuators are perhaps the most commonly used [35,36]. In such systems, the pressure may serve to directly load a flexible structure [18], or can be used indirectly to induce local instabilities in structured materials that manifest as macroscopic motions [37]. More recent actuation mechanisms have explored the use of shape memory alloys [38] and electroactive polymers [39], with the promise of application in soft robotics [40].

Inspiration for the type of control we seek to achieve in flexible manipulators can be drawn from various biological systems [41]. Invoking a broad analogy, ours is an invertebrate structure that needs to be bent in a desired way. Studies on the locomotion of snakes [42,43], the flexibility of octopus tentacles and the dexterity of elephant trunks have influenced the design of various biomimetic robotic systems [44,45], some of which have been commercialized [46,47]. As revealed by the materials and actuation mechanisms we consider here, our goal is not biomimicry. Rather, we seek to realize shapes and deformations that can be used, if desired, to replicate natural functions.

Besides the implications for flexible robotics, the control problem we consider is directly relevant to the analysis and design of guyed columns and cable supported structures [48,49]. Our work can also be interpreted in the context of curve approximation, since we seek to approximate a design curve (desired shape) by certain elastica solutions [50], with the feature of the approximation parameters having meaningful physical interpretations. Such curve approximation problems are commonly known as "rationalization" in the literature on computer-aided design and have applications in manufacturing processes such as robotic hot blade cutting [51].

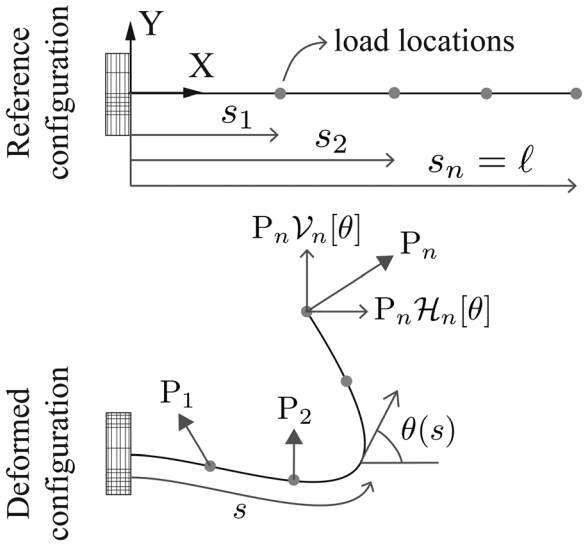

Fig. 2 Illustration of the choice of coordinates and the loading configuration for the problem of computing the deformation of an elastica discussed in Sec. 2

2 The Forward Problem

We devote this section to detailing the forward problem defining the deformation of an elastica subjected to a collection of concentrated loads. The forward problem will serve as a point of departure for discussing the shape control problem in Sec. 3.

2.1 Kinematics and Equilibrium. We consider an elastica of length ℓ and bending modulus B that is clamped at its left end. It is subjected to n point loads $\{P_i \in \mathbb{R}\}_{i=1}^{n}$, with the load P_i acting at a distance s_i measured along the length of the beam from the clamped end as illustrated in Fig. 2. For definiteness, we set $s_0 = 0$ and assume that $s_0 < s_1 < s_2 < \ldots < s_n = \ell$. The case where the nth load acts at $s_n < \ell$ is easily accommodated, for instance, by considering $n+1$ loads and setting $s_{n+1} = \ell$ with $P_{n+1} = 0$. Assuming the elastica to be straight when unloaded, we describe its deformed configuration with the map $s \mapsto \theta(s)$ that measures the inclination of the tangent to the centerline of the beam as a function of the arc-length parameter $s \in [0, \ell]$. This choice of coordinate helps to automatically incorporate the familiar inextensibility constraint. Adopting a Cartesian system of coordinates (x, y) in which the origin coincides with the clamped end and the horizontal axis with the centerline of the beam in its reference configuration, the coordinates of a point at a distance s along the centerline in the deformed configuration are given by

$$(x(s), y(s)) = \int_0^s (\cos\theta(t),\ \sin\theta(t))\, dt \tag{1}$$

We denote the direction cosines of the jth load by the functionals $(\mathcal{H}_j[\theta], \mathcal{V}_j[\theta])$, where the dependence on θ permits considering loads whose inclinations are configuration-dependent. For example, $(\mathcal{H}_j[\theta], \mathcal{V}_j[\theta]) = (\cos\mu, \sin\mu)$ for a load acting at a constant inclination μ measured from the horizontal, while $(\mathcal{H}_j[\theta], \mathcal{V}_j[\theta]) = (-\sin\theta(s_j), \cos\theta(s_j))$ for a follower load that remains normal to

the beam at s_j. In Sec. 4, we provide these functionals for the case of tendon loads. In the ensuing discussion, however, we do not assume a specific form for the inclination functionals.

Balancing moments at a point $s \in (s_i, s_{i+1})$, we get

$$B\theta'(s) = \sum_{j=i+1}^{n} P_j((x(s_j) - x(s))\mathcal{V}_j[\theta] - (y(s_j) - y(s))\mathcal{H}_j[\theta])$$

where $\theta'(s) \triangleq d\theta(s)/ds$ measures the local curvature at s and $0 \le i < n$. Differentiating the equation above with respect to the parameter s and invoking the relationship $(x'(s), y'(s)) = (\cos\theta(s), \sin\theta(s))$ implied by Eq. (1), we arrive at the force balance

$$B\theta''(s) = \sum_{j=i+1}^{n} P_j(\mathcal{V}_j[\theta]\cos\theta(s) - \mathcal{H}_j[\theta]\sin\theta(s)) = 0 \quad \text{for } s_i < s < s_{i+1} \text{ and } 0 \le i < n \tag{2}$$

which are augmented with the boundary conditions

$$\theta(0) = \theta'(\ell) = 0 \tag{3}$$

signifying that the end $s = 0$ is clamped while the end $s = \ell$ is moment-free.

Multiplying Eq. (2) by an admissible variation $s \mapsto \delta\theta(s)$ of θ, integrating by parts, and noting the boundary conditions implied by Eq. (3) on θ and $\delta\theta$, we get the principle of virtual work

$$\begin{aligned} G(\theta; \delta\theta) \triangleq & \int_{s=0}^{\ell} B\theta'\delta\theta'\, ds \\ & + \sum_{i=0}^{n-1}\sum_{j=i+1}^{n} \int_{s_i}^{s_{i+1}} P_j(\mathcal{H}_j[\theta]\sin\theta - \mathcal{V}_j[\theta]\cos\theta)\delta\theta\, ds \\ & = 0 \quad \forall\, \delta\theta \text{ admissible} \end{aligned} \tag{4}$$

It is evident from the terms $\cos\theta$ and $\sin\theta$ appearing in the integrand that the dependence of G on θ in Eq. (4) is nonlinear. The direction cosines $\{(\mathcal{H}_j[\theta], \mathcal{V}_j[\theta])\}_j$ may serve as additional sources of nonlinearity.

2.2 Finite Element Approximation. Equation (4) is the point of departure for computing finite element approximations to θ. We adopt a piecewise linear discretization for θ and resolve the resulting nonlinear system of equations with a Newton algorithm. To this end, we compute the directional derivative of $G(\theta; \delta\theta)$ along $s \mapsto \Delta\theta(s)$ as

$$\begin{aligned} DG(\theta;\delta\theta)\cdot\Delta\theta \triangleq & \frac{d}{d\varepsilon}|_{\varepsilon=0} G(\theta + \varepsilon\Delta\theta; \delta\theta) \\ = & \int_{s=0}^{\ell} B\delta\theta'\Delta\theta'\, ds + \sum_{i=1}^{n-1}\sum_{j=i+1}^{n}\int_{s_i}^{s_{i+1}} \mathrm{P}_j\big(\mathcal{H}_j[\theta]\cos\theta + \mathcal{V}_j[\theta]\sin\theta\big)\delta\theta\Delta\theta ds \\ & + \sum_{i=1}^{n-1}\sum_{j=i+1}^{n}\int_{s_i}^{s_{i+1}} P_j\Big(\mathcal{H}_j'(\theta;\Delta\theta)\sin\theta - \mathcal{V}_j'(\theta;\Delta\theta)\cos\theta\Big)\delta\theta ds \end{aligned} \tag{5}$$

where we have used the shorthand $(\mathcal{H}_j'(\theta;\Delta\theta), \mathcal{V}_j'(\theta;\Delta\theta))$ for the directional derivatives $D(\mathcal{H}_j[\theta], \mathcal{V}_j[\theta])\cdot\Delta\theta$. For example, $(\mathcal{H}_j'(\theta;\Delta\theta), \mathcal{V}_j'(\theta;\Delta\theta))$ equals (0, 0) for a nonfollower load (e.g., dead load), while

$$(\mathcal{H}_j'(\theta;\Delta\theta), \mathcal{V}_j'(\theta;\Delta\theta)) = -(\cos\theta(s_j),\ \sin\theta(s_j))\Delta\theta(s_j) \tag{6}$$

for a follower that remains normal to the beam at s_j.

A consistent linearization $\Delta\theta \mapsto \mathcal{L}G(\theta;\delta\theta)(\Delta\theta)$ of Eq. (4) suitable for a Newton-algorithm now follows as

$$\mathcal{L}G(\theta;\delta\theta)(\Delta\theta) \triangleq G(\theta;\delta\theta) + DG(\theta;\delta\theta)\cdot\Delta\theta \tag{7}$$

Hence, starting from an initial guess $s \mapsto \theta_0(s)$, we adopt an iterative procedure where at the kth iteration, we compute the solution increment $\Delta\theta_k$ by resolving the affine system

$$\mathcal{L}G(\theta_k;\delta\theta)(\Delta\theta_k) = 0 \quad \forall\, \delta\theta \text{ admissible} \tag{8}$$

coupled with the Dirichlet boundary condition $\Delta\theta_k(0) = 0$. Restricting the solution iterate θ_k, the admissible variations $\delta\theta$ and the solution increment $\Delta\theta_k$ to belong to the finite element space transforms Eq. (8) into a linear system of algebraic equations. Then with $\Delta\theta_k$ at hand, we update the solution guess to $\theta_{k+1} = \theta_k + \Delta\theta_k$ and continue iterating in this way until the residual G is deemed to be sufficiently small.

2.3 Remarks. Observe that since the finite element residual vector and stiffness matrix furnished by Eq. (7) are in general configuration-dependent, it is necessary to reassemble them after each solution iteration. In practice, neither the linearization $\mathcal{L}G$ in Eq. (7) nor the solution increment $\Delta\theta$ in Eq. (8) need to be computed accurately; the satisfaction of equilibrium conditions and the termination of the numerical algorithm only require that G be evaluated well. In particular, it is beneficial to drop terms of the form $P_j(\mathcal{H}_j'(\theta;\Delta\theta)\sin\theta - \mathcal{V}_j'(\theta;\Delta\theta)\cos\theta)$ appearing in the integrand in Eq. (5) since their inclusion can result in a dense and nonsymmetric stiffness matrix. This is in fact the case for tendon-driven loads discussed in Sec. 4. Due to the piecewise nature of the force balance statement, which manifests as partitioned integrals in Eq. (4), we ensure that the points $s_1, \ldots, s_n$ are included in the set of nodes in the finite element mesh in order to simplify the choice of quadrature rules for numerically evaluating the integrals appearing in G and its linearization. Finally, we mention that the straightforward Newton algorithm that we adopt here is unsuitable for computing solutions when there is a possibility of snap-through or buckling phenomena. In such cases, arc-length methods and path-following strategies are more appropriate. Since none of the examples considered in this paper involve such instabilities, we omit a discussion of these alternative algorithms and refer to Ref. [52] instead.

2.4 Examples and Comparisons With the Literature. We show a few examples in Fig. 3 comparing our finite element approximations of elastica solutions with those available in the literature. In Figs. 3(*a*)–3(*c*), we compare our calculations with elliptic integral-based solutions from Refs. [4], [5], and [53], respectively. We present similar comparisons for the case of tendon loads (Sec. 4). While there is no limitation in our numerical algorithm on either the number or the locations of the loads, elliptic integral-based solutions are invariably derived for the case of end loads. Elliptic integral solutions for the case of multiple loads can be found in Ref. [5] for example. We have compared our calculations with these solutions as well but omit them here for the sake of brevity. Instead, Fig. 3(*d*) shows a comparison of our finite element calculations with the shooting method [10]. We have included the case of a follower load in Fig. 3(*c*) solely for the purpose of verifying the correctness of our implementation. In particular, we do not consider such loads to be a feasible means of operating flexible manipulators [54].

We conclude this section by mentioning that the general formulation for the forward problem in Eq. (4) and its linearization using Eq. (5) helps to reproduce a variety of solutions that have been derived in the literature. The benefit of such generality will become more evident when we consider the case of tendon loads in Sec. 4.

3 Shape Control Through Load Optimization

The stage is now set for us to introduce the shape control problem. From the outset, we assume that the number of loads n, their

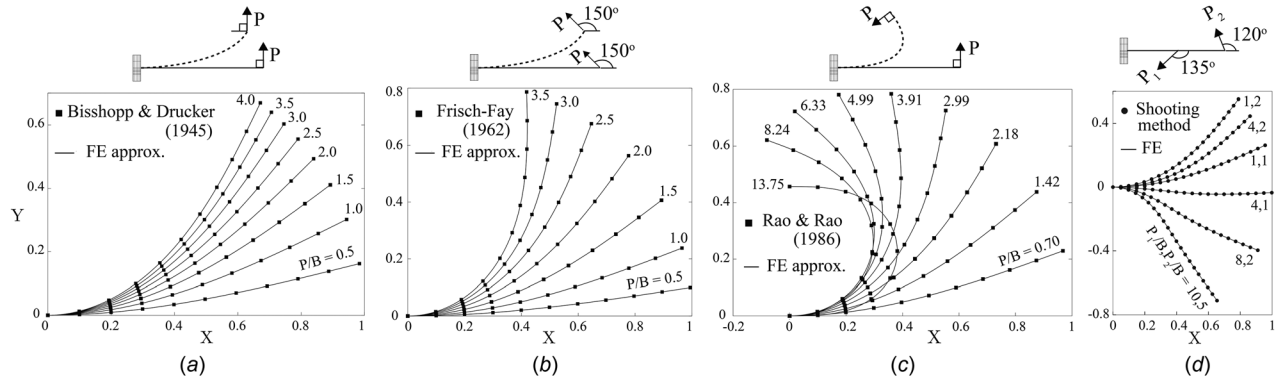

Fig. 3 Plots (*a*)–(*c*) compare our finite element approximations of elastica solutions with elliptic integral-based solutions derived in the literature. Plot (*d*) shows a comparison with an alternative numerical method.

locations $\{s_j\}_{j=1}^n$ and the nature of the loads in the form of the inclination functionals $\{(\mathcal{H}_j, \mathcal{V}_j)\}_{j=1}^n$ are specified. We presume these to be the result of design considerations and operational constraints. Then, given a desired configuration $s \mapsto \theta_{\mathrm{d}}(s)$ for the elastica, our goal in this section is to identify a set of loads $\mathbf{P} = (P_1, \ldots, P_n) \in \mathbb{R}^n$ that yields an equilibrium solution $\theta_{\mathbf{P}}$ to approximate θ_{d} well. The manipulator design specifications, i.e., the parameters n, $\{s_i\}_i$ and $\{(\mathcal{H}_i, \mathcal{V}_i)\}_i$ remain unchanged irrespective of the prescription for θ_{d}. Instead, the only control available to approximate the desired configuration is the set of loads $\mathbf{P}$.

The subscript $\mathbf{P}$ appearing in $\theta_{\mathbf{P}}$, not used in Sec. 2, is introduced here to serve as a reminder of the dependence of the elastica solution on the set of loads, which is the basis for the shape control problem. We note that the desired configuration can also be specified in the form of coordinate functions $s \mapsto (x_{\mathrm{d}}(s), y_{\mathrm{d}}(s))$, from where it is straightforward to deduce θ_{d} using the relationship $(x'_{\mathrm{d}}(s), y'_{\mathrm{d}}(s)) = (\cos\theta_{\mathrm{d}}(s), \sin\theta_{\mathrm{d}}(s))$.

3.1 Objective Functional. By way of posing the question of finding $\mathbf{P}$ as an optimization problem, we introduce the objective functional

$$J(\mathbf{P}) \triangleq \frac{1}{2}\int_{s=0}^{\ell} (\theta_{\mathbf{P}}(s) - \theta_{\mathrm{d}}(s))^2 \, ds \tag{9}$$

where the dependence of $J(\mathbf{P})$ on $\mathbf{P}$ is implicit in $\theta_{\mathbf{P}}$. Evidently, $J(\mathbf{P})$ is the squared L^2-norm of the difference $(\theta_{\mathbf{P}} - \theta_{\mathrm{d}})$ between the realized and the desired solutions computed over $[0, \ell]$. Our goal is hence to identify $\mathbf{P}$ as a minimizer of J. Although each

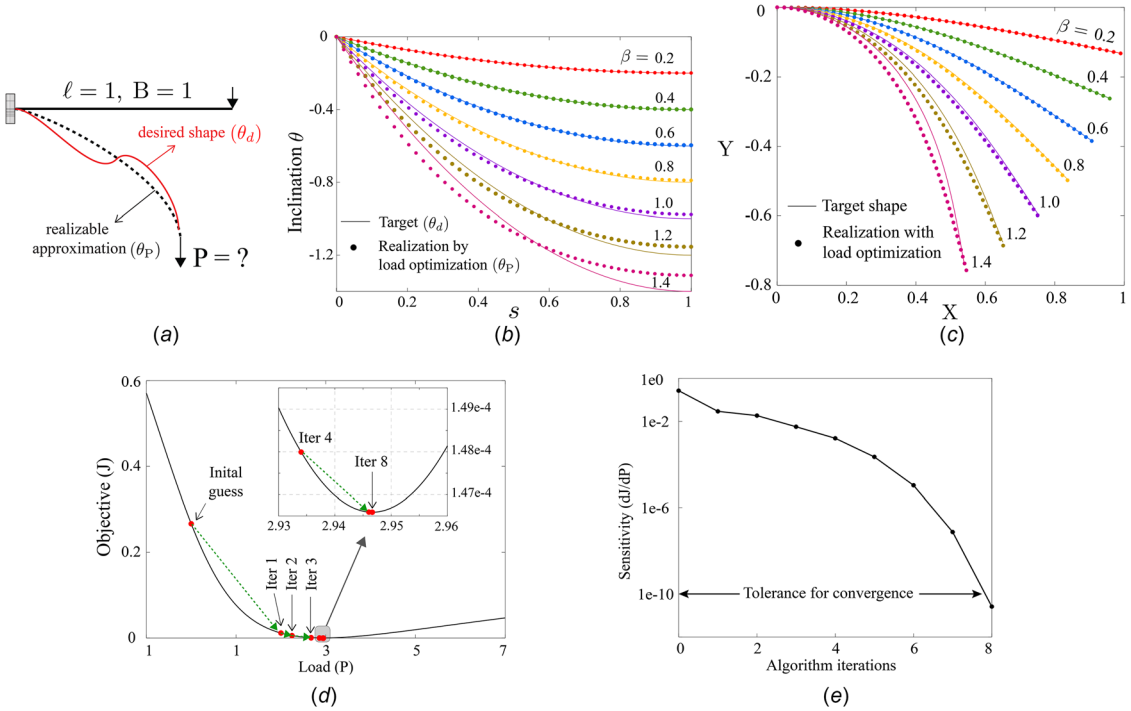

Fig. 4 With the manipulator shown in (*a*) designed with one end vertical load, we seek a load *P* that approximates a given target deformation (θ_{d}) as an elastica solution. Plots (*b*) and (*c*) show the approximation achieved by computing optimal loads as outlined in Sec. 3.2 to approximate target inclinations of the form $\theta_{\mathrm{d}} = \beta s(s-2)$. While (*b*) compares the functions $\theta_{\mathrm{d}}(s)$ and $\theta_{\mathrm{P}}(s)$, (*c*) compares the corresponding set of deformations. For the specific case of $\beta = 1$, details of the convergence of the load optimization scheme to a minimizer of the objective functional are shown in (*d*) and (*e*). The algorithm terminates after 8 iterations, when the sensitivity $|dJ/dP|$ becomes smaller than the specified tolerance 10^{-10}.

choice for θ_{d} defines a new objective, for notational simplicity, we have omitted denoting the dependence of J on θ_{d} explicitly.

The form of the objective in Eq. (9) is chosen for its simplicity. Needless to say, other definitions are certainly possible. In particular, we draw attention to the fact that although the dependence of J on $\theta_{\mathbf{P}}$ is quadratic in Eq. (9), its dependence on $\mathbf{P}$ may not be (see Fig. 4(*d*)). For this reason, we cannot make claims on the existence/uniqueness of minimizers for J and rely on a posteriori comparison of $\theta_{\mathbf{P}}$ and θ_{d} to infer if the identified solution $\mathbf{P}$ is indeed a minimizer.

3.2 Optimal Loads as a Stationary Point of *J*. Seeking a stationary point of J, we formally set $\partial J(\mathbf{P})/\partial P_k = 0$ for each $k = 1, \ldots, n$. More succinctly, we require that

$$\nabla_{\mathbf{P}} J(\mathbf{P}) \triangleq \left(\frac{\partial J(\mathbf{P})}{\partial P_1}, \ldots, \frac{\partial J(\mathbf{P})}{\partial P_n} \right) = 0$$

Employing the definition of J from Eq. (9), we have

$$\frac{\partial J(\mathbf{P})}{\partial P_k} = \int_{s=0}^{\ell} (\theta_{\mathbf{P}}(s) - \theta_{\mathrm{d}}(s)) \underbrace{\frac{\partial \theta_{\mathbf{P}}(s)}{\partial P_k}}_{\alpha_k(s)} \, ds \tag{10}$$

The derivative $\alpha_k(s) \triangleq \partial \theta_{\mathbf{P}}(s)/\partial P_k$ appearing in Eq. (10) is the *sensitivity* of the elastica solution to the load P_k, i.e., α_k is a measure of how the elastica solution changes when the load P_k is perturbed. In summary, with $\boldsymbol{\alpha} \triangleq (\alpha_1, \ldots, \alpha_n)$, we seek $\mathbf{P} \in \mathbb{R}^n$ that satisfies

$$\nabla_{\mathbf{P}} J(\mathbf{P}) = \int_{s=0}^{\ell} (\theta_{\mathbf{P}}(s) - \theta_{\mathrm{d}}(s)) \, \boldsymbol{\alpha}(s) \, ds = 0 \tag{11}$$

The integrand in Eq. (11) depends on $\mathbf{P}$ through the elastica solution $\theta_{\mathbf{P}}$ as well as through the set of sensitivities $\boldsymbol{\alpha}$. We have omitted explicitly indicating the dependence of $\boldsymbol{\alpha}$ on $\mathbf{P}$, unlike in the case of $\theta_{\boldsymbol{P}}$, to avoid indicial clutter.

With Eq. (11) at hand, the question of identifying the optimal load $\mathbf{P}$ reduces to a problem in numerical optimization. In principle, a simple gradient descent scheme will suffice—starting from an initial guess $\mathbf{P}_0$, iteratively improve solution guesses using updates of the form $\mathbf{P}_{m+1} = \mathbf{P}_m - \gamma_m \nabla_{\mathbf{P}} J(\mathbf{P}_m)$, where γ_m is an iteration dependence scale factor chosen to be sufficiently small to ensure that $J(\mathbf{P}_{m+1}) \leq J(\mathbf{P}_m)$. It is also appealing to choose a Newton algorithm to resolve Eq. (11), but such a scheme requires expensive calculations of higher order sensitivities (derivatives of the form $\partial^2 \theta_{\mathbf{P}}/\partial P_k \partial P_j$). We resort to a quasi-Newton method instead, where the Hessian of J is computed approximately using its gradients. Specifically, we use the Broyden–Fletcher–Goldfarb–Shanno algorithm implemented in the Toolkit for Advanced Optimization library [55]. We mention the possibility of adopting derivative-free algorithms such as the Nedler–Mead method for minimizing J, in which case the gradient $\nabla_{\mathbf{P}} J(\mathbf{P})$, and consequently the sensitivities $\boldsymbol{\alpha}$, is not required. Nevertheless, we prefer derivative-based methods for their superior convergence properties and the guarantees they provide [56].

Evaluating the objective J and its gradients $\nabla_{\mathbf{P}} J$ at solution iterates for $\mathbf{P}$ realized during iterative minimization evidently requires computing the elastica solution and its sensitivities at these loads. At a given solution guess $\mathbf{P}$, Sec. 2 details the procedure for computing a numerical approximation of $\theta_{\mathbf{P}}$ satisfying Eq. (5). We take up the task of computing the corresponding set of sensitivities $\boldsymbol{\alpha}$ next.

3.3 Load Sensitivity of Elastica Solutions. Differentiating the force balance Eq. (3) for $\theta_{\mathbf{P}}$ over the section (s_i, s_{i+1}) with respect to the load P_k, we get

$$\begin{aligned} B \frac{\partial (\theta''_{\mathbf{P}}(s))}{\partial P_k} &= \frac{\partial}{\partial P_k} \left(\sum_{j=i+1}^{n} P_j \left(\mathcal{H}_j[\theta_{\mathbf{P}}] \sin \theta_{\mathbf{P}}(s) - \mathcal{V}_j[\theta_{\mathbf{P}}] \cos \theta_{\mathbf{P}}(s) \right) \right) \\ &= \sum_{j=i+1}^{n} \delta_{jk} \left(\mathcal{H}_j[\theta_{\mathbf{P}}] \sin \theta_{\mathbf{P}}(s) - \mathcal{V}_j[\theta_{\mathbf{P}}] \cos \theta_{\mathbf{P}}(s) \right) \\ &\quad + \sum_{j=i+1}^{n} P_j \left(\mathcal{H}_j[\theta_{\mathbf{P}}] \cos \theta_{\mathbf{P}}(s) + \mathcal{V}_j[\theta_{\mathbf{P}}] \sin \theta_{\mathbf{P}}(s) \right) \frac{\partial \theta_{\mathbf{P}}(s)}{\partial P_k} \\ &\quad + \sum_{j=i+1}^{n} P_j \left(\frac{\partial \mathcal{H}_j[\theta_{\mathbf{P}}]}{\partial P_k} \sin \theta_{\mathbf{P}}(s) - \frac{\partial \mathcal{V}_j[\theta_{\mathbf{P}}]}{\partial P_k} \cos \theta_{\mathbf{P}}(s) \right) \end{aligned} \tag{12}$$

where δ_{jk} is the Kronecker delta symbol. To simplify Eq. (12), we first use the fact that the derivatives of $\theta_{\mathbf{P}}$ with respect to s and P_k commute. Consequently, $\partial(\theta''_{\mathbf{P}})/\partial P_k = \alpha''_k$. Next, the terms $\partial(\mathcal{H}_j[\theta_{\mathbf{P}}], \mathcal{V}_j[\theta_{\mathbf{P}}])/\partial P_k$ appearing in the last row of Eq. (12) have the useful characterization

$$\frac{\partial (\mathcal{H}_j[\theta_{\mathbf{P}}], \mathcal{V}_j[\theta_{\mathbf{P}}])}{\partial P_k} = \left(\mathcal{H}'_j(\theta_{\mathbf{P}}; \alpha_k), \mathcal{V}'_j(\theta_{\mathbf{P}}; \alpha_k) \right) \tag{13}$$

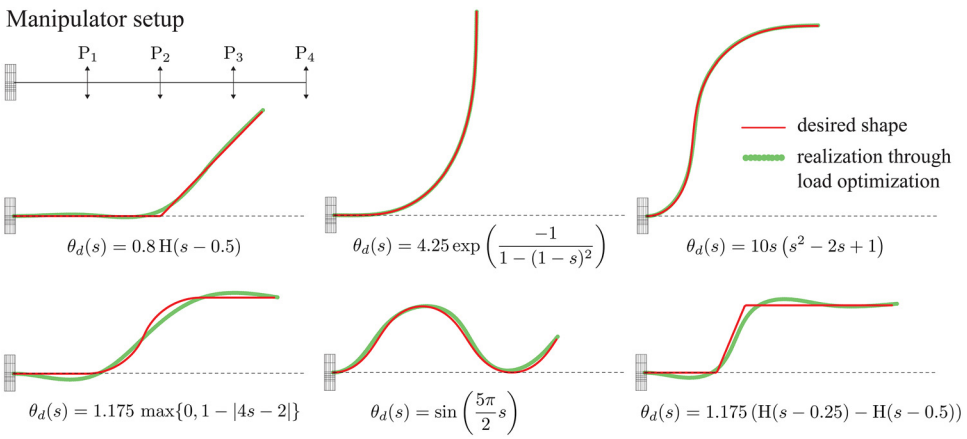

Fig. 5 Demonstrating the capability of a manipulator designed with four vertical loads P_{1-4} to approximate a series of different target deformations by optimizing the set of loads. The target inclinations are indicated alongside each example.

and represent the *sensitivities of the inclination functionals*.

Proceeding to simplify Eq. (12), we now have

$$B\alpha_k'' = \sum_{j=i+1}^{n} \delta_{jk}(\mathcal{H}_j[\theta_\mathbf{P}]\sin\theta_\mathbf{P} - \mathcal{V}_j[\theta_\mathbf{P}]\cos\theta_\mathbf{P}) + \sum_{j=i+1}^{n} P_j(\mathcal{H}_j[\theta_\mathbf{P}]\cos\theta_\mathbf{P} + \mathcal{V}_j[\theta_\mathbf{P}]\sin\theta_\mathbf{P})\alpha_k + \sum_{j=i+1}^{n} P_j(\mathcal{H}_j'(\theta_\mathbf{P};\alpha_k)\sin\theta_\mathbf{P} - \mathcal{V}_j'(\theta_\mathbf{P};\alpha_k)\cos\theta_\mathbf{P}) \tag{14}$$

over the interval (s_i, s_{i+1}) and for each $0 \le i < n$. The boundary conditions for α_k follow from Eq. (4) as

$$\alpha_k(0) = \alpha_k'(\ell) = 0. \tag{15}$$

A few remarks are in order at this point. First, since $(\mathcal{H}_j(\theta_\mathbf{P};\alpha_k), \mathcal{V}_j(\theta_\mathbf{P};\alpha_k))$ is linear in the second argument α_k, we note that Eq. (14) is a linear differential equation for α_k. This is in contrast to the nonlinear nature of Eq. (2) defining $\theta_\mathbf{P}$. Second, it is apparent from Eq. (14) that the sensitivity of the elastica solution to the load P_k depends, in general, on the entire set of loads $(P_1, \ldots, P_n)$, the set of direction cosines $\{(\mathcal{H}_j, \mathcal{V}_j)\}_j$, as well as on the set of their derivatives $\{(\mathcal{H}_j', \mathcal{V}_j')\}_j$. This observation reveals that $\boldsymbol{\alpha}$ effectively quantifies the relationship between the load sensitivity of a flexible manipulator and its design parameters.

We adopt a finite element method to approximate the sensitivities $\boldsymbol{\alpha}$ as well. Here, we just provide the weak form G_k corresponding to Eq. (14) that is required in a finite element implementation to approximate the sensitivity component α_k. Choosing $\delta\alpha$ to be an admissible variation of α_k and by following manipulations similar to those in Sec. 2, we get

$$G_k(\alpha_k;\delta\alpha) \triangleq \int_{s=0}^{\ell} B\alpha_k'\delta\alpha'\,ds + \sum_{i=0}^{n-1}\sum_{j=i+1}^{n} \delta_{jk}\int_{s_i}^{s_{i+1}} (\mathcal{H}_j[\theta_\mathbf{P}]\sin\theta_\mathbf{P} - \mathcal{V}_j[\theta_\mathbf{P}]\cos\theta_\mathbf{P})\delta\alpha\,ds + \sum_{i=0}^{n-1}\sum_{j=i+1}^{n}\int_{s_i}^{s_{i+1}} P_j(\mathcal{H}_j[\theta_\mathbf{P}]\cos\theta_\mathbf{P} + \mathcal{V}_j[\theta_\mathbf{P}]\sin\theta_\mathbf{P})\alpha_k\,\delta\alpha\,ds + \sum_{i=0}^{n-1}\sum_{j=i+1}^{n}\int_{s_i}^{s_{i+1}} P_j(\mathcal{H}_j'(\theta_\mathbf{P};\alpha_k)\sin\theta_\mathbf{P} - \mathcal{V}_j'(\theta_\mathbf{P};\alpha_k)\cos\theta_\mathbf{P})\,\delta\alpha\,ds$$

Since G_k is linear in both its arguments, no additional linearization procedures such as those required for G are necessary.

3.4 Numerical Experiments. We examine the performance of the proposed load-optimization scheme with the help of numerical experiments. In all the examples, we assume the elastica to be of unit length ($\ell = 1$) and set $B = 1$ (in appropriate units).

3.4.1 Controlling a Cantilever. In the first example shown in Fig. 4, we consider an elastica that is subjected to a vertical end load. We seek to approximate solutions of the form $\theta_\mathrm{d} = \beta s(s-2)$ for a range of values of the parameter β. These set of target solutions and the corresponding set of elastica shapes for $\beta = 0.2, 0.4, \ldots, 1.4$ are shown in solid lines in Figs. 4(*b*) and 4(*c*), respectively. The solutions $\theta_\mathbf{P}$ realized by the load optimization scheme are indicated by circular markers in these figures. In each case, we find that the realized solutions approximate the desired ones reasonably well, and from Fig. 4(*c*), we find that the tip of the elastica follows the target location accurately. The result in Fig. 4(*b*) can also be interpreted from the perspective of approximating polynomials of the form $\beta s(s-2)$ by functions represented using elliptic integrals, with the fitting parameter being the load magnitude. It is evident from Fig. 4(*c*) why the approximation deteriorates for larger values of β—as β grows, so does the end rotation of the beam, and such shapes are simply not realizable with our simplistic manipulator consisting of one vertical end load.

For the case $\theta_\mathrm{d} = s(s-2)$, i.e., $\beta = 1$, Figs. 4(*d*) and 4(*e*) show details of the iterations to convergence in the optimization scheme. As indicated in Fig. 4(*d*), we start from the trivial initial guess $P = 0$. At each iteration, the computed sensitivity automatically guides the solution toward progressively smaller values of the objective. The gradient of the objective realized at each iteration is plotted in Fig. 4(*e*). At the eighth iteration, we find that $|dJ/dP|$ is smaller than the preset tolerance 10^{-10}, indicating that the Broyden–Fletcher–Goldfarb–Shanno algorithm has found a stationary point of J at $P \approx 2.947$. In the process, the objective is reduced from 0.267 to 1.466×10^{-4}.

3.4.2 A Four-Load Manipulator. Figure 5 shows a manipulator designed with four equally spaced vertical loads used to approximate six different target shapes. We find that the realized solutions match the target deformations reasonably well in all cases. Improving the approximations further requires changing the design of the manipulator, i.e., the number, locations, and/or the type of loadings. This example helps to highlight that having sufficiently many loads is critical in realizing a rich *workspace*, i.e., a diverse set of realizable deformations. Examples involving the Heaviside function (H) also convey the importance of approximating target solutions rather than attempting to reproduce them. To wit, these target deformations have sharp kinks and are therefore not even admissible elastica solutions. Nevertheless, the optimization scheme identifies loads that approximate these deformations well. Finally, we note that while it is possible to identify optimal loads using naïve sampling strategies in the case of one, or even two loads, heuristic search schemes become prohibitively expensive as the number of loads increases. This should be contrasted with the optimization algorithm proposed here, which converges within 10–15 iterations in most of our examples.

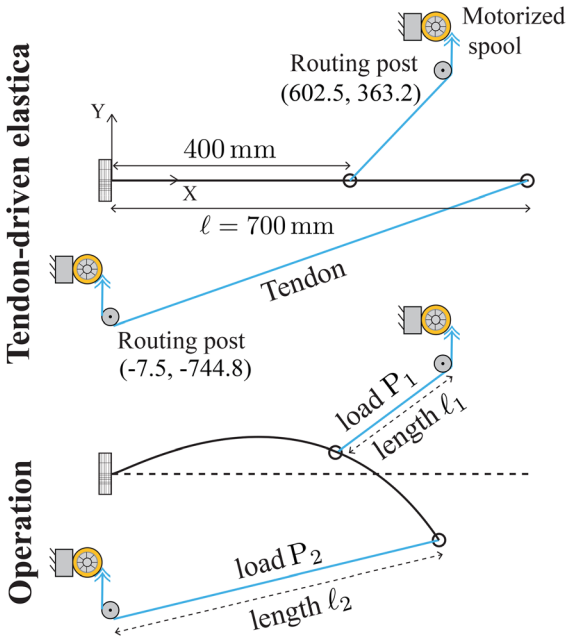

Fig. 6 Experimental setup for demonstrating shape control in a manipulator actuated using a pair of tendons routed through fixed posts. All coordinates mentioned in the figure are in mm.

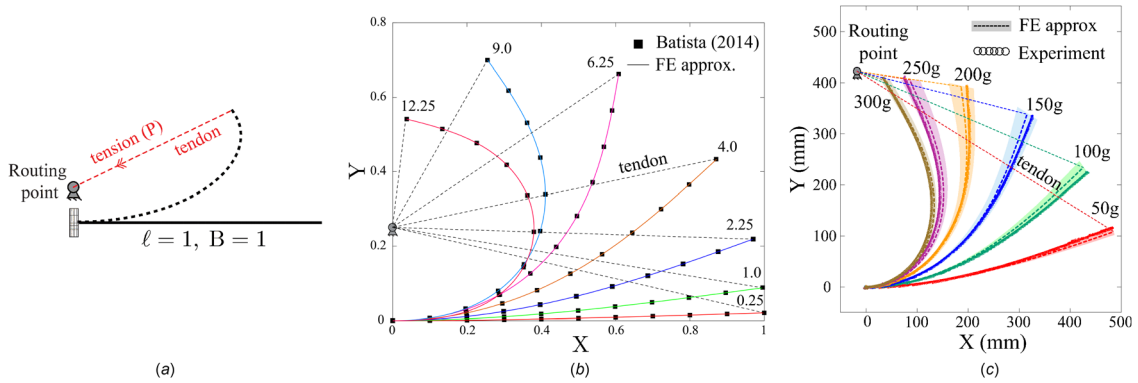

Fig. 7 A comparison of the finite element approximation of an elastica loaded by a tendon shown in (*a*) with a Jacobi-elliptic integral solution from the literature is shown in (*b*). The plot in (*c*) compares experimental measurements of the deformation with numerical solutions while allowing for a 5% uncertainty in the load.

4 Tendon-Driven Manipulators

Tendon-driven elastic arms constitute an important class of robotic manipulators. Besides their high degree of flexibility, their adaptability across multiple length scales while relying essentially on the same operating principle adds to their appeal. This is in contrast to traditional manipulators composed of rigid links and actuators, which become progressively more challenging to design and expensive to fabricate at smaller length scales. This section is aimed at demonstrating shape control for a simplistic class of tendon-driven manipulators using the framework of load optimization.

4.1 Specialization of the Forward Problem. We consider an elastica loaded by n tendons attached at points $\{s_i\}_{i=1}^{n}$ along its length and assume that the tendons are routed through the fixed points $\{(x_i, y_i)\}_{i=1}^{n}$, see Figs. 1 and 6. The inclination functionals for the jth load are given by

$$\big(\mathcal{H}_j[\theta], \mathcal{V}_j[\theta]\big) = \frac{\big(x_j - x(s_j), y_j - y(s_j)\big)}{\sqrt{\big(x_j - x(s_j)\big)^2 + \big(y_j - y(s_j)\big)^2}} \tag{16}$$

which is simply the unit vector pointing from the attachment point $(x(s_j), y(s_j))$ to the routing point (x_j, y_j). The dependence of the right hand side on θ in Eq. (16) is implicit in the relationship $(x(s_j), y(s_j)) \triangleq \int_{s=0}^{s_j} (\cos\theta(s), -\sin\theta(s))\, ds$. The directional derivatives of these inclinations, required in the linearization of the weak form and for computing the sensitivities, follow as:

$$\begin{cases} \mathcal{H}_j'(\theta; \Delta\theta) = -(Dx(s_j) \cdot \Delta\theta)\,(y_j - y(s_j))^2 / r^{3/2} \\ \mathcal{V}_j'(\theta; \Delta\theta) = -(Dy(s_j) \cdot \Delta\theta)\,(x_j - x(s_j))^2 / r^{3/2} \\ \text{where } r = \big((x_j - x(s_j))^2 + (y_j - y(s_j))^2\big)^{1/2} \end{cases}$$

and the directional derivatives of $(x(s_j), y(s_j))$ are given by $D(x(s_j), y(s_j)) \cdot \Delta\theta = \int_0^{s_j} (-\sin\theta(s),\ \cos\theta(s)) \Delta\theta(s)\, ds$.

In contrast to the simple form of the inclinations in the cases of loads acting at a constant angle to a datum or to the beam, Eq. (16) reveals a nonlinear functional dependence between the inclination of a tendon load and the elastica solution. In this sense, Eq. (16) fully justifies the general framework introduced for the forward problem in Sec. 2.

Figure 7(*b*) compares the Jacobi elliptic integral solution derived in Refs. [48] and [49] for the case of a tendon load acting at the end of an elastica with our finite element calculations. Besides the specific form of the inclination functionals given by Eq. (16), all other aspects of our solution algorithm are identical to those used for the examples in Sec. 2. Figure 7(*c*) compares predictions from our calculations and an experiment in which a beam is loaded quasi-statically by a tendon attached to its end. The tendon is loaded in 50 g increments and the deformed shapes of the beam are measured using a laser scanner mounted on a portable coordinate measuring machine (Romer Absolute Arm). We additionally include an envelope of computed solutions while allowing for a 5% variation around the nominal applied load to account for uncertainties in the experiment, including friction between the tendon and its routing post. The comparisons reveal a good match between the model and the experiments. Figure 7(*c*) also helps to highlight the distinction between tendon loads and follower loads. While Eq. (16) clearly reveals that tendon loads are configuration-dependent, their inclination to the beam is not assumed a priori, but is computed as part of the solution. This is in contrast to follower loads which are (somehow) constrained to remain at a fixed inclination to the deforming beam, see Ref. [54] for a review of attempts to realize such loadings in practice.

4.2 Shape Control. Figure 6 shows a schematic consisting of a flexible polycarbonate arm of length $\ell = 700$ mm actuated by a pair of tendons attached at $s_1 = 400$ mm and $s_2 = 700$ mm. The tendons are routed through fixed posts whose coordinates are mentioned in the figure. For each given target deformation, the optimization algorithm computes the tensions in the two tendons required to approximate the desired beam shape. Figure 8 shows the optimal solutions computed to approximate target deformations having inclination functions of the form $\theta_d = \eta\, s(s^2 + \beta_1 s + \beta_0)$ for different values of the parameter η. In these calculations, we use the tensions computed for smaller values of η as the initial guess for computing loads at larger η. Such an incremental optimization strategy is important in practice because the objective functional may have multiple stationary points and/or there may be

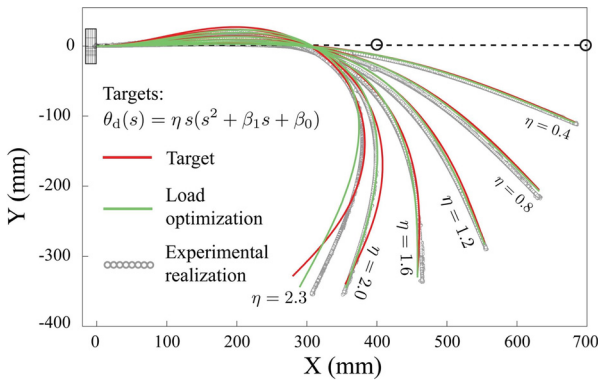

Fig. 8 Progressive approximation of a one-parameter set of target deformations achieved using the load optimization algorithm for the setup in Fig. 6. Experimental measurements approximate the optimized solution well.

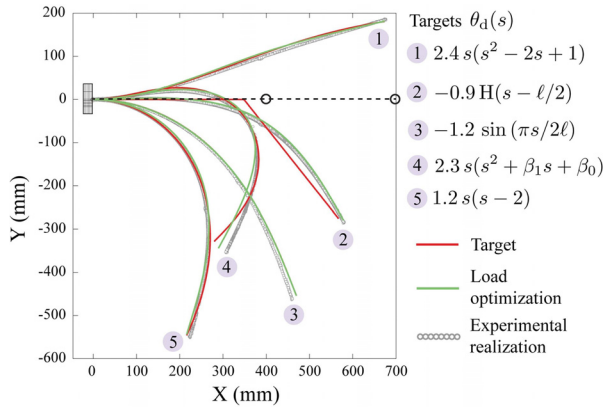

Fig. 9 More examples and experiments demonstrating shape control for the manipulator in Fig. 6 to approximate varied target solutions

multiple equilibrium solutions for the same set of tendon loads. Figure 9 similarly demonstrates the manipulator approximating various target deformations. Each specification for the target θ_d defines a new objective functional J. Yet, nothing besides the tensions in the tendons can be altered to approximate the desired shape. Nevertheless, we find that the computed solutions approximate even exaggerated deformations of the arm quite well.

An important consideration with tendon manipulators is the restriction that each tendon can only transmit tensile loads. In the context of the setup in Fig. 6, this implies the constraints $P_1, P_2 \geq 0$ since negative loads causes slack in tendons. Such constraints can be incorporated within the load optimization scheme as "trust regions," for instance. Despite these restrictions, the examples in Figs. 8 and 9 clearly demonstrate that tendon manipulators can help realize a rich workspace.

4.3 Experimental Realization. Toward validating our load optimization approach for manipulating tendon-driven arms in a controlled manner, we have designed a rudimentary setup based on Fig. 6 and uses a pair of stepper motors to operate the tendon spools. The arm is loaded by simply reeling in and reeling out the tendons.

In principle, the tensions computed by the optimization algorithm can be imposed through the motors by using a load cell for each tendon. As a simpler alternative, we directly use the active lengths of the tendons, which is the distance between the attachment points on the deformed beam and the routing posts, to deduce the number of rotations required for the spools attached to the motors. In Fig. 6, these active lengths are indicated by ℓ_1 and ℓ_2. Hence the optimization algorithm presumes the actuation to be tendon-load-controlled, while the actuation in the experiment is tendon-length-controlled. In performing such a transformation of variables ($P_1 \mapsto \ell_1$ and $P_2 \mapsto \ell_2$), we implicitly assume a locally injective relationship between the active length of a tendon and the tension it bears. This assumption, though valid in our experiments, can be violated when there are snap-through instabilities for instance. The idea of load-controlled computations followed by length-controlled manipulation of tendon-arms makes the manipulator inexpensive by avoiding the need for sensitive load cells, and quite robust by not requiring careful quantification of friction between tendons and their routing posts.

In summary, given a target deformation:

(i) we compute the necessary tensions P_1, P_2 using the load optimization algorithm;
(ii) transform the tensions P_1, P_2 to the active lengths ℓ_1, ℓ_2 for the tendons;
(iii) deduce the number of turns of the spools required to achieve the computed active lengths ℓ_1, ℓ_2;
(iv) and slowly (approximately quasi-statically) operate the motors to reel in or reel out each tendon.

Observe that such a predictive framework is an open loop system, i.e., there is no feedback from the arm to the loading mechanism.

Figures 8 and 9 show the experimentally realized beam shapes measured using a laser scanner. These measurements are expected to lie close to the optimized solutions, which appears to be the case in all the examples. Small deviations are certainly present and we suspect that improving the accuracy of our motorized length control mechanism, which is roughly 10 mm in the setup used here, will help to reduce the mismatch. Comparing the experimental measurements to the target solutions in the figures reflects the effectiveness of the load optimization algorithm for realizing controlled manipulation of the arm while operating within the given design constraints.

5 Concluding Remarks

We have introduced a framework for realizing controlled manipulation of flexible beams by optimizing the loads applied and demonstrated its versatility with the help of varied experiments. Generalizing the forward problem by considering inclinations to be functionals of the solution, resolving the resulting nonlinear differential equations with a finite element method, and identifying optimal loads to approximate target deformations using solution sensitivities to guide minimization procedures, are all crucial aspects of our approach. The resulting mechanics-based quantitative framework for realizing controlled manipulation, albeit in the simple context of planar beams, should be contrasted with the more ubiquitous statistical training methods that arguably reduce the control problem to a data-fitting exercise.

We note a few observations on the performance of the load optimization scheme based on our numerical experiments. Without exception, we find that requiring the target solution and the admissible set of elastica solutions to satisfy identical boundary conditions drastically reduces the approximation error. Our calculations show that the elastica solution is often less sensitive to loads applied close to the clamped end when compared to loads applied farther away. This is perhaps to be expected as well. Nevertheless, this observation has important consequences. It suggests that (optimized) loads applied close to the clamped end are likely to have large magnitudes. As a remedy, the objective functional can be modified to penalize large loads at the expense of admitting an increase in the approximation error. A second consequence of the contrast in load sensitivities is that the optimization problem can become ill-conditioned and may therefore require special numerical algorithms to ensure fast convergence. We also find that including a (non-negative) weight factor in the definition of the objective functional in Eq. (9), say as $J(\mathbf{P}) = \int_{s=0}^{\ell} w(s)\,(\theta_{\mathbf{P}}(s) - \theta_d(s))^2\,ds$, can help in improving local approximations of the target solution.

Preliminary results analyzing tendon-driven manipulators, including the ones studied here, provide encouraging evidence of the practical applicability of the load control scheme. We mention that it is immediately possible to consider a wider variety of loading scenarios, starting with the inclusion of moment loads in tendon manipulators where cables are attached away from the centerline, as well as consider shape manipulation by controlling electromagnetic interactions. The objective functional can also be tailored, for instance, to realize a desired position for the tip of the manipulator rather than attempting to match a target shape for the beam. A mathematical analysis of the load optimization scheme, aimed at analyzing the existence and (non)uniqueness of solutions, inspecting the stability of computed solutions, and deriving a priori estimates for the error between target and realizable shapes, also warrants immediate attention. Such an analysis may shed light on the relationship between the workspace of a

manipulator and its design parameters, and in turn suggest informed choices for objective functionals as well.

While our excursion here has been restricted to the case of planar manipulators, it is conceivable that the ideas introduced will extend to realizing shape control in three-dimensional rods [22]. It is of course necessary to identify rod models capable of accommodating large displacements and rotations [57]. In closing, we mention that there are many aspects relevant to practical operation of flexible manipulators that we have not paid heed to. This includes accounting for contact interactions with an external environment [58], compliance control relevant in medical device applications where the external environment may be soft tissues [59], or even vibration damping in the beam when imposing the computed set of loads dynamically [60].

Acknowledgment

This work was sponsored by the ISRO-IISc Space Technology Cell. The authors thank Dr. Manish Trikha (Indian Space Research Organization) for helpful discussions.

Funding Data

- Indian Space Research Organisation (ISTC/MME/RSR/0386).

References

[1] Polygerinos, P., Wang, Z., Galloway, K., Wood, R., and Walsh, C., 2015, "Soft Robotic Glove for Combined Assistance and At-Home Rehabilitation," Rob. Auton. Syst., **73**, pp. 135–143.
[2] Degani, A., Choset, H., Zubiate, B., Ota, T., and Zenati, M., 2008, "Highly Articulated Robotic Probe for Minimally Invasive Surgery," IEEE International Conference on Robotics and Automation (ICRA), Orlando, FL, May 15–19, pp. 3273–3276.
[3] Antman, S., 2006, *Nonlinear Problems of Elasticity* (Applied Mathematical Sciences), Springer, New York.
[4] Bisshopp, K., and Drucker, D., 1945, "Large Deflection of Cantilever Beams," Q. Appl. Math., **3**(3), pp. 272–275.
[5] Frisch-Fay, R., 1962, *Flexible Bars*, Butterworths, London.
[6] Navaee, S., and Elling, R., 1992, "Equilibrium Configurations of Cantilever Beams Subjected to Inclined End Loads," ASME J. Appl. Mech., **59**(3), pp. 572–579.
[7] Zhang, A., and Chen, G., 2013, "A Comprehensive Elliptic Integral Solution to the Large Deflection Problems of Thin Beams in Compliant Mechanisms," ASME J. Mech. Rob., **5**(2), p. 021006.
[8] Batista, M., 2014, "Analytical Treatment of Equilibrium Configurations of Cantilever Under Terminal Loads Using Jacobi Elliptical Functions," Int. J. Solids Struct., **51**(13), pp. 2308–2326.
[9] Wang, C., 1981, "Large Deflections of an Inclined Cantilever With an End Load," Int. J. Nonlinear Mech., **16**(2), pp. 155–164.
[10] Wang, C., and Kitipornchai, S., 1992, "Shooting-Optimization Technique for Large Deflection Analysis of Structural Members," Eng. Struct., **14**(4), pp. 231–240.
[11] Wang, C., Lam, K., He, X., and Chucheepsakul, S., 1997, "Large Deflections of an End Supported Beam Subjected to a Point Load," Int. J. Nonlinear Mech., **32**(1), pp. 63–72.
[12] Shvartsman, B., 2013, "Analysis of Large Deflections of a Curved Cantilever Subjected to a Tip-Concentrated Follower Force," Int. J. Nonlinear Mech., **50**, pp. 75–80.
[13] Watson, L., and Wang, C., 1981, "A Homotopy Method Applied to Elastica Problems," Int. J. Solids. Struct., **17**(1), pp. 29–37.
[14] Zhang, X., and Yang, J., 2005, "Inverse Problem of Elastica of a Variable-Arc-Length Beam Subjected to a Concentrated Load," Acta Mech. Sin., **21**(5), pp. 444–450.
[15] Hinze, M., Pinnau, R., Ulbrich, M., and Ulbrich, S., 2008, *Optimization With PDE Constraints. Mathematical Modelling: Theory and Applications*, Springer, Dordrecht, The Netherlands.
[16] Haslinger, J., 2003, *Introduction to Shape Optimization: Theory, Approximation, and Computation*, Vol. 7, SIAM, Philadelphia, PA.
[17] Shoup, T., and McLarnan, C., 1971, "On the Use of the Undulating Elastica for the Analysis of Flexible Link Mechanisms," J. Eng. Ind., **93**(1), pp. 263–267.
[18] Wilson, J., and Snyder, J., 1988, "The Elastica With End-Load Flip-Over," ASME J. Appl. Mech., **55**(4), pp. 845–848.
[19] Gravagne, I. A., and Walker, I. D., 2002, "Manipulability, Force, and Compliance Analysis for Planar Continuum Manipulators," IEEE Trans. Rob. Autom., **18**(3), pp. 263–273.
[20] Li, C., and Rahn, C., 2002, "Design of Continuous Backbone, Cable-Driven Robots," ASME J. Mech. Des., **124**(2), pp. 265–271.
[21] Trivedi, D., Lotfi, A., and Rahn, C., 2008, "Geometrically Exact Models for Soft Robotic Manipulators," IEEE Trans. Rob., **24**(4), pp. 773–780.
[22] Rucker, C., and Webster, R., 2011, "Statics and Dynamics of Continuum Robots With General Tendon Routing and External Loading," IEEE Trans. Rob., **27**(6), pp. 1033–1044.
[23] Camarillo, D., Milne, C., Carlson, C., Zinn, M., and Salisbury, K., 2008, "Mechanics Modeling of Tendon-Driven Continuum Manipulators," IEEE Trans. Rob., **24**(6), pp. 1262–1273.
[24] Webster, R. J., III., and Jones, B. A., 2010, "Design and Kinematic Modeling of Constant Curvature Continuum Robots: A Review," Int. J. Rob. Res., **29**(13), pp. 1661–1683.
[25] Chirikjian, G., 1994, "Hyper-Redundant Manipulator Dynamics: A Continuum Approximation," Adv. Rob., **9**(3), pp. 217–243.
[26] Challamel, N., Kocsis, A., and Wang, C., 2015, "Discrete and Non-Local Elastica," Int. J. Nonlinear Mech., **77**, pp. 128–140.
[27] Wang, C., 2015, "Longest Reach of a Cantilever With a Tip Load," Eur. J. Phys., **37**(1), p. 012001.
[28] Mochiyama, H., Watari, M., and Fujimoto, H., 2007, "A Robotic Catapult Based on the Closed Elastica and Its Application to Robotic Tasks," IEEE/RSJ International Conference on Intelligent Robots and Systems (IROS), San Diego, CA, Oct. 29–Nov. 2, pp. 1508–1513.
[29] Patricio, P., Adda-Bedia, M., and Ben Amar, M., 1999, "An Elastica Problem: Instabilities of an Elastic Arch," Phys. Sect. D, **124**(1–3), pp. 285–295.
[30] Plaut, R., and Virgin, L., 2009, "Vibration and Snap-Through of Bent Elastica Strips Subjected to End Rotations," ASME J. Appl. Mech., **76**(4), p. 041011.
[31] Armanini, C., Dal Corso, F., Misseroni, D., and Bigoni, D., 2017, "From the Elastica Compass to the Elastica Catapult: An Essay on the Mechanics of Soft Robot Arm," Proc. R. Soc. A, **473**(2198), p. 20160870.
[32] Griner, G., 1984, "A Parametric Solution to the Elastic Pole-Vaulting Pole Problem," ASME J. Appl. Mech., **51**(2), pp. 409–414.
[33] Zhang, Y., Wang, Y., Li, Z., Huang, Y., and Li, D., 2007, "Snap-Through and Pull-in Instabilities of an Arch-Shaped Beam Under an Electrostatic Loading," J. Microelectromech. Syst., **16**(3), pp. 684–693.
[34] Rus, D., and Tolley, M. T., 2015, "Design, Fabrication and Control of Soft Robots," Nature, **521**(7553), pp. 467–475.
[35] Mosadegh, B., Polygerinos, P., Keplinger, C., Wennstedt, S., Shepherd, R., Gupta, U., Shim, J., Bertoldi, K., Walsh, C., and Whitesides, G., 2014, "Pneumatic Networks for Soft Robotics That Actuate Rapidly," Adv. Funct. Mater., **24**(15), pp. 2163–2170.
[36] Connolly, F., Walsh, C., and Bertoldi, K., 2017, "Automatic Design of Fiber-Reinforced Soft Actuators for Trajectory Matching," Proc. Natl. Acad. Sci., **114**(1), pp. 51–56.
[37] Yang, D., Mosadegh, B., Ainla, A., Lee, B., Khashai, F., Suo, Z., Bertoldi, K., and Whitesides, G., 2015, "Buckling of Elastomeric Beams Enables Actuation of Soft Machines," Adv. Mater., **27**(41), pp. 6323–6327.
[38] Huang, W., 2002, "On the Selection of Shape Memory Alloys for Actuators," Mater. Des., **23**(1), pp. 11–19.
[39] Bar-Cohen, Y., 2004, "Electroactive Polymer (EAP) Actuators as Artificial Muscles: Reality, Potential, and Challenges," *SPIE Press Monographs*, SPIE, Bellingham, WA.
[40] Trivedi, D., Rahn, C., Kier, W., and Walker, I., 2008, "Soft Robotics: Biological Inspiration, State of the Art, and Future Research," Appl. Bionics Biomech., **5**(3), pp. 99–117.
[41] Kier, W., and Smith, K., 1985, "Tongues, Tentacles and Trunks: The Biomechanics of Movement in Muscular-Hydrostats," Zool. J. Linnean Soc., **83**(4), pp. 307–324.
[42] Hirose, S., 1993, *Biologically Inspired Robots: Snake-like Locomotors and Manipulators*, Vol. 1093, Oxford University Press, Oxford, UK.
[43] Cicconofri, G., and DeSimone, A., 2015, "A Study of Snake-like Locomotion Through the Analysis of a Flexible Robot Model," Proc. R. Soc. A, **471**(2184), p. 20150054.
[44] Hannan, M., and Walker, I., 2003, "Kinematics and the Implementation of an Elephant's Trunk Manipulator and Other Continuum Style Robots," J. Rob. Syst., **20**(2), pp. 45–63.
[45] Laschi, C., Cianchetti, M., Mazzolai, B., Margheri, L., Follador, M., and Dario, P., 2012, "Soft Robot Arm Inspired by the Octopus," Adv. Rob., **26**(7), pp. 709–727.
[46] Immega, G., and Antonelli, K., 1995, "The KSI Tentacle Manipulator," IEEE International Conference on Robotics and Automation, Nagoya, Japan, May 21–27, pp. 3149–3154.
[47] Buckingham, R., 2002, "Snake Arm Robots," Ind. Rob., **29**(3), pp. 242–245.
[48] Yau, J., 2010, "Closed-Form Solutions of Large Deflection for a Guyed Cantilever Column Pulled by an Inclination Cable," J. Mar. Sci. Technol., **18**(1), pp. 130–136.
[49] Batista, M., 2015, "Large Deflection of Cantilever Rod Pulled by Cable," Appl. Math. Model., **39**(10–11), pp. 3175–3182.
[50] Brander, D., Gravesen, J., and Nørbjerg, T., 2017, "Approximation by Planar Elastic Curves," Adv. Comput. Math., **43**(1), pp. 25–43.
[51] Søndergaard, A., Feringa, J., Nørbjerg, T., Steenstrup, K., Brander, D., Graversen, J., Markvorsen, S., Bærentzen, A., Petkov, K., Hattel, J., Clausen, K., Jensen, K., Knudsen, L., and Kortbek, J., 2016, "Robotic Hot-Blade Cutting," *Robotic Fabrication in Architecture, Art and Design*, Springer, Cham, Switzerland, pp. 150–164.
[52] Wriggers, P., 2008, *Nonlinear Finite Element Methods*, Springer, Berlin.
[53] Rao, N., and Rao, V., 1986, "On the Large Deflection of Cantilever Beams With End Rotational Load," Z. Angew. Math. Mech., **66**(10), pp. 507–509.
[54] Elishakoff, I., 2005, "Controversy Associated With the so-Called Follower Forces: Critical Overview," Appl. Mech. Rev., **58**(2), pp. 117–142.

[55] Munson, T., Sarich, J., Wild, S., Benson, S., and McInnes, L., 2017, "Tao 3.8 Users Manual," Mathematics and Computer Science Division, Argonne National Laboratory, Lemont, IL.
[56] Nocedal, J., and Wright, S., 2006, *Numerical Optimization* (Springer Series in Operations Research and Financial Engineering), Springer, New York.
[57] Simo, J., 1985, "A Finite Strain Beam Formulation. the Three-Dimensional Dynamic Problem—Part I," Comput. Methods Appl. Mech. Eng., **49**(1), pp. 55–70.
[58] Chen, J., and Li, H., 2011, "On an Elastic Rod Inside a Slender Tube Under End Twisting Moment," ASME J. Appl. Mech, **78**(4), p. 041009.
[59] Mahvash, M., and Dupont, P., 2011, "Stiffness Control of Surgical Continuum Manipulators," IEEE Trans. Rob., **27**(2), pp. 334–345.
[60] Okubo, S., and Tortorelli, D., 2004, "Control of Nonlinear, Continuous, Dynamic Systems Via Finite Elements, Sensitivity Analysis, and Optimization," Struct. Multidiscip. Optim., **26**(3–4), pp. 183–199.